

MIT Open Access Articles

Experimental measurements of ICRF minority-heated fast-ion distributions on Alcator C-Mod

The MIT Faculty has made this article openly available. **Please share** how this access benefits you. Your story matters.

Citation: Bader, A., R.S. Granetz, R.R. Parker, P.T. Bonoli, I.H. Hutchinson, J. Sears, and S.J. Wukitch. "Experimental measurements of ion cyclotron range of frequency minority-heated fast-ion distributions on Alcator C-Mod." *Nuclear Fusion* 52, no. 9 (September 1, 2012): 094019.

As Published: <http://dx.doi.org/10.1088/0029-5515/52/9/094019>

Publisher: IOP Publishing

Persistent URL: <http://hdl.handle.net/1721.1/84062>

Version: Author's final manuscript: final author's manuscript post peer review, without publisher's formatting or copy editing

Terms of use: Creative Commons Attribution-Noncommercial-Share Alike 3.0



Experimental Measurements of ICRF Minority-heated Fast-Ion Distributions on Alcator C-Mod

A. Bader 1), R.S. Granetz 1), R.R. Parker 1), P.T. Bonoli 1), I.H. Hutchinson 1), J. Sears 2), S.J. Wukitch 1)
1) MIT Plasma Science and Fusion Center, Cambridge, MA 02139,
USA 2) Los Alamos National Laboratory, Los Alamos, NM, 87545

ICRH (Ion Cyclotron Resonance Heating) is the primary auxiliary heating on the Alcator C-Mod tokamak and is commonly used on other devices, and is planned for use on ITER. The RF-power density on C-Mod is above 5 MW/m^3 providing for a unique opportunity to study wave-particle effects in the high RF power per particle regime. Minority heating produces a highly energetic tail in the minority distribution function which is measured using a Compact Neutral Particle Analyzer. In this paper, we present the measurements of the fast-ion spectrum between 200 keV and 2 MeV, compiled over an entire experimental campaign. We also estimate the effective tail temperatures for the fast-ion distribution. We find that the fast-ion distribution is less energetic and less dense with increasing electron density; is more energetic with increasing plasma current; and is more dense but has no measurable change in energy with increasing RF power. Some possible explanations for these findings are discussed.

I. INTRODUCTION

Ion Cyclotron Range of Frequency (ICRF) minority heating is a common tool on current fusion devices and is planned to be present on future devices [1]. In order to predict the performance of ICRF on future devices, and to do transport analysis on current devices, it is crucial to understand the wave damping physics [2] and to experimentally measure the energetic ion tail produced by ICRF waves [3, 4]. Diagnostics using neutral particle analysis have provided important measurements of the fast-ion distribution on many devices [5–10]. Recently, the novel concept of detecting neutral particles using solid-state diode detectors has lowered the size and cost of neutral particle diagnostics and permitted an improvement in diagnostic capabilities [11, 12].

The Alcator C-Mod tokamak is well-suited for experimental research of ICRF generated fast-ion tails [13]. High input power (up to 5 MW) in the minority-heating regime, combined with a compact tokamak ($\sim 1 \text{ m}^3$ plasma volume), produces extremely high ICRF power densities, up to 5 MW/m^3 when averaged over the entire tokamak volume, and likely as high as $20\text{-}30 \text{ MW/m}^3$ if the power is deposited over a fairly small resonance layer. Additionally, C-Mod produces plasmas where the RF power/particle is ~ 10 times higher than what can be obtained on other tokamaks, such as JET. Plasma current up to 1.2 MA is sufficient to confine fast ions up to 2 MeV and, the high magnetic fields (5.4 T in normal operation) produce small ion gyroradii even for fast-ions. A 1 MeV fast-ion has an ion gyroradius of $\sim 2.7 \text{ cm}$ in C-Mod. An orbit for a highly energetic fast-ion near the resonance layer is shown in Figure 1.

The presence of very high energy fast-ions in minority-heated plasmas has been observed on other tokamaks, such as JET using both neutral particle analysis and gamma ray spectroscopy [14–16]. These results indicate that minority-heating can produce an extremely energetic tail, several 100 times the plasma temperature at

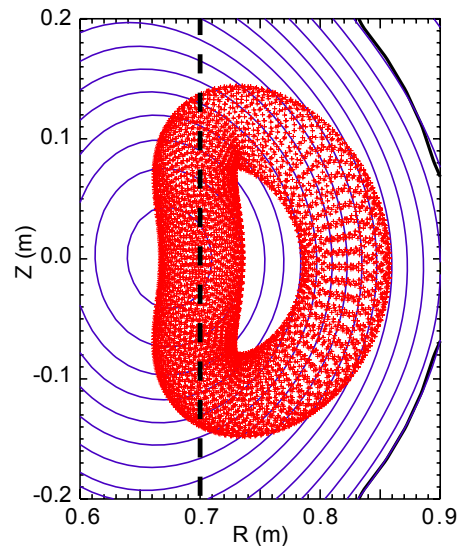


FIG. 1: Poloidal projection of the orbit of a 3 MeV proton with banana tips near the resonance layer of a 1 MA plasma on Alcator C-Mod. The thick vertical dashed line represents the estimated location of the ICRF resonance.

localized pitch angles and radial locations. As indicated by the results in JET, the best sightline to view energetic particles is a vertical sightline viewing from the top of the tokamak at or near the resonance layer. This sightline has a line-integrated view of all the trapped particles with banana tips on the resonance layer, and thus obtains a high signal-to-noise at the expense of information about which magnetic flux-surface the fast-ion neutralizes on.

This paper provides the first systematic measurements of the fast-ion distribution in the high RF-power density regime. We present the first measurements of the dependences of the fast-ion distribution spectra and effective temperature on electron density, plasma current and RF power in this regime. Additional research, using

advanced simulation techniques has been done [17] and will be presented in a forthcoming publication. However, in this paper we attempt to interpret the experimental results using simple models and heuristic arguments where possible.

The layout of the paper is as follows. Section II describes the Compact Neutral Particle Analyzer used for the experimental measurements. Section III shows the scaling of the fast-ion distribution with electron density, plasma current, ICRF power, and magnetic field. Section IV describes the methodology used to convert the detector signal into an estimate of the fast-ion distribution in the plasma. Section V calculates an effective tail temperature of the fast-ion distribution and shows how the effective temperature scales with electron density, plasma current and RF power. Section VI provides discussion for the results and describes possible reasons for the scalings seen in the experimental measurements, and discusses some areas for future research.

II. CNPA DIAGNOSTIC AND EXPERIMENTAL MEASUREMENTS

Alcator C-Mod has had two compact neutral particle analyzers (CNPAs). The diagnostics employ biased silicon-diode detectors that detect individual fast neutral particles. Fast-neutrals are created from ICRF minority-heated ions that neutralize and escape the plasma. The signal from the detectors pass through shaping electronics and are digitized at 10 MHz. The diagnostic located at F-Port is described in detail in [12]. In this paper we use measurements obtained from a new diagnostic that was installed at J-Port that uses AXUV HS1-20 silicon diode detectors from International Radiation Detectors (IRD), each looking through individual adjustable apertures. A schematic of the locations of the detector footprints on the midplane, the ICRF antennas, and the plasma limiters are shown in a top down plan view of the C-Mod tokamak in Figure 2.

Both diagnostics view vertically down from the top of the machine and the diagnostic viewing sightlines intersect magnetic field lines at near perpendicular angles. Thus the detectors are sensitive only to particles that have low local values of v_{\parallel} , i.e. trapped particles near their turning points. The new HS1-20 detectors have active regions deep enough ($200 \mu\text{m}$) to detect fast particles up to 2 MeV. Consequently, electronic gain has been adjusted to take advantage of the improved energy range. The deeper active region makes the detectors more susceptible to both low-level photon noise and spurious counts from high energy x-rays. The background photon noise sets the upper limit for the aperture, and makes it difficult to obtain measurements in highly radiative plasmas, such as H-modes. The photon limitation is in contrast to other neutral particle or hard x-ray diagnostics that are limited by pulse pile-up. In addition to the energy range, the spatial viewing range has been in-

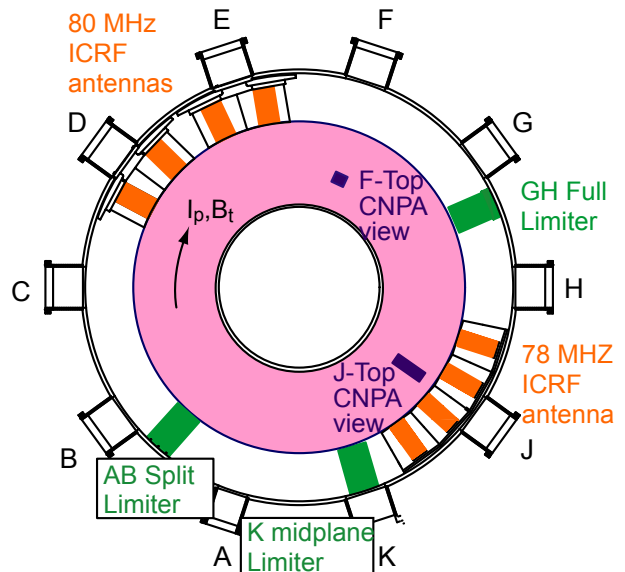


FIG. 2: Top down schematic of the Alcator C-Mod vessel.

creased. Whereas the old F-Port detectors have a very limited viewing range in major radius (68 - 71 cm), the new detectors view from major radii of 70 - 78 cm. It should be noted that the original location of the F-Port detectors was chosen to have a view of the diagnostic neutral beam. However, the beam has since been pivoted, and currently neither the J-Top or F-Top detectors have a view of the beam. The location of three of the sightlines on J-Top, showing the outermost and innermost views, are shown in Figure 3.

Experimental measurements are made by counting single impact events from fast-neutrals impinging on the detector. The signal from a single event is electronically shaped into a Gaussian with a $1 \mu\text{s}$ width. The electronics and 10 MHz digitization is unchanged from [12] and will not be further described here. The CNPA regularly detects fast neutrals up to 1.5 MeV, and occasionally up to 2 MeV. Previous work on Alcator by Rost [18] detected only low energy particles when viewing from the outboard midplane. Further work by Tang [19] detected particles up to 400 keV, but was prevented from measuring higher energy neutrals due to the detector and electronics characteristics. For the research presented here, the diagnostic was calibrated using thick-target scattered ions between 500 keV and 1.1 MeV on two separate occasions. There was no detectable degradation of detector performance over a single campaign.

A typical plasma discharge with 3 MW of RF power is shown in Figure 4. In this discharge, it can be shown that the RF power produces both a rise in electron temperature and a signal on the CNPA, indicating that the ICRF waves are producing a minority tail that is depositing some of its energy into the bulk plasma.

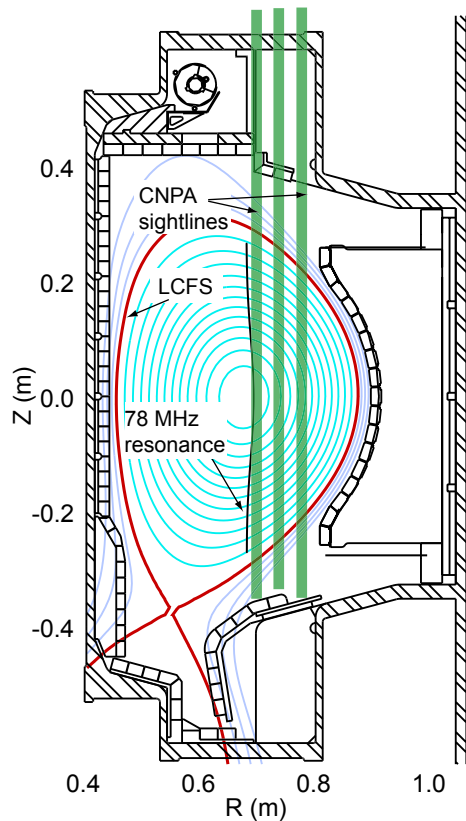


FIG. 3: Sightlines for the CNPA views plotted over an EFIT reconstructed magnetic equilibrium are shown along with an estimation of the ICRF resonance location for normal operation.

III. SCALING OF FAST-ION DISTRIBUTION WITH PLASMA PARAMETERS

The fast-ion distribution is dependent on various plasma parameters. Among these are magnetic field, electron density, ICRF power, ICRF frequency, plasma current and hydrogen fraction. In addition, the signal received by the detector is also dependent on the density of electron-donor species, which is not well known. Of the known parameters, the vast majority of C-Mod plasmas are operated at normal operating toroidal fields between 5.2 and 5.4 T and normal operating ICRF frequencies of 78, 80 and 80.5 MHz for J, D and E antennas respectively. The hydrogen fraction is high at the beginning of a campaign, but after the first month of operation it settles into a range between 0.05-0.1. In general, the margin of error on the H to D ratio is ± 0.03 . In the normal operating field and frequencies, the innermost J-Port CNPA channel ($R = 70$ cm) views very near to the ICRF resonance layer, and has the largest signal-to-noise of any channel, and thus the best signal levels.

In this section we analyze the dependence of the CNPA signal at the detector on electron density, ICRF power and plasma current. We analyze all plasma discharges

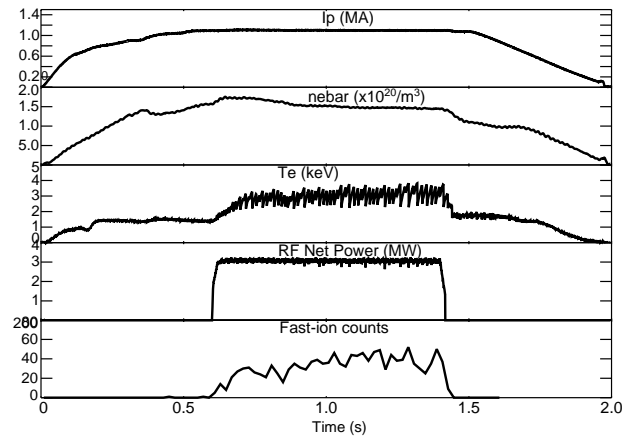


FIG. 4: Sample discharge with traces of plasma current, line averaged electron density, electron temperature, RF power, and fast-ion counts.

in a campaign that have normal operating fields, normal ICRF frequencies, and that have hydrogen fractions below 10%. We divide the flattop region of each discharge into 20 ms time bins, and categorize each time bin with the average values of three plasma parameters of interest: electron density, RF power and plasma current. Then we examine the dependence of the fast-neutral distribution on each plasma parameter while holding the other two constant. Because of the method of data gathering, we are limited to presenting data from the operating parameters that are most commonly used on C-Mod in order to obtain sufficient statistics for analysis. However, we do not distinguish between different plasma shapings, different topology, or different operating regimes such as High Confinement (H)-Modes. Unfortunately, there is very limited data in certain areas of interest, such as low power (< 1 MW). The parameter space available for analysis is presented in Figure 5.

In the distributions presented below, the effective temperature of the fast-ion distribution (T_{eff}) is estimated by examining the slope of the fast-ion distribution. In this section only qualitative statements are made about the fast-ion distribution. In Section V quantitative estimates of the fast-ion temperatures will be presented. The discharges shown here present the fast-ion count rate in counts per eV per second per cm^2 per steradian. The factor of cm^{-2} steradian $^{-1}$ represents the etendue given by the aperture area multiplied by the solid angle subtended. The factor is necessary to allow for direct comparisons of different aperture sizes used in different discharges.

More energetic distributions with higher fast-ion densities are found at lower electron densities. Heuristically this occurs because the ICRF power is deposited over a smaller number of particles and therefore, the temperature of the fast ion distribution varies inversely with the density of the minority species. Additionally, the ion slowing down time scales inversely with electron density, and at lower densities a neutralized fast-ion is more likely

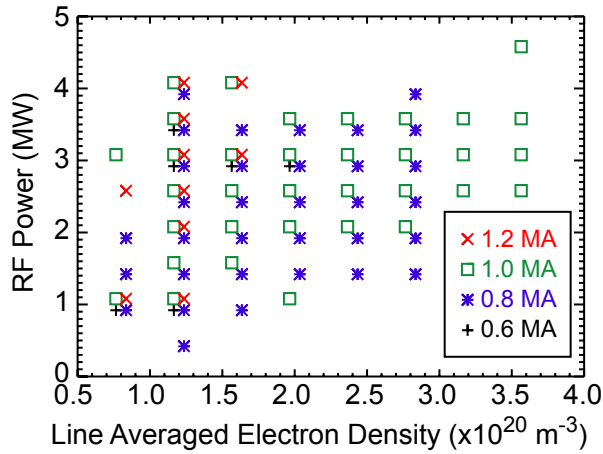


FIG. 5: Alcator C-Mod parameter space with sufficient data for analysis. Values are plotted for line averaged electron density between 0.5 and 4.0×10^{20} RF power between 1 and 5 MW, and plasma currents of: 0.6 MA, $q_{95} \approx 6.0$, (black +); 0.8 MA, $q_{95} \approx 4.5$, (*); 1.0 MA, $q_{95} \approx 3.4$, (\square) and 1.2 MA, $q_{95} \approx 3.0$, (\times).

to exit the plasma without being reionized. All these factors contribute to produce a more energetic distribution and increased detector counts at low electron densities. Figure 6 shows the results of the CNPA signal as a function of energy for different electron densities.

It is more difficult to understand the dependences of the fast-ion distribution on plasma current and RF power. We find that as plasma current is raised, both the number of fast-ion counts and the apparent temperature of the distribution increases. These dependences are shown in Figure 8 where we plot the fast-ion distribution for various plasma currents. We also discover an interesting trend when examining the dependence of the distribution on RF power. The distribution has low energy and low count rate density at power levels below about 1.5 MW. However, at power levels above 2 MW we see no further increase of T_{eff} and only a small increase in fast-ion density (Figure 7). There is a saturation of tail temperature above a certain power level, and additional ICRF power does not contribute to a measurable increase in the temperature of the fast-ion distribution.

We also show the dependence of the fast-ion distribution on magnetic field and find that the location of peak signal varies as a function of magnetic field and tends to appear slightly outboard of the calculated location of the resonance. In Figure 9 we plot three discharges with different magnetic field values, all with only a single operating antenna. The paramagnetic effect of the plasma tends to push the location of the resonance outboard ~ 2 cm near the plasma center.

The fast-ions viewed on the CNPA sightlines are seen to be unaffected by plasma sawteeth. This is likely due to the fact that plasma sawteeth are not likely to redistribute trapped ions above a certain energy threshold

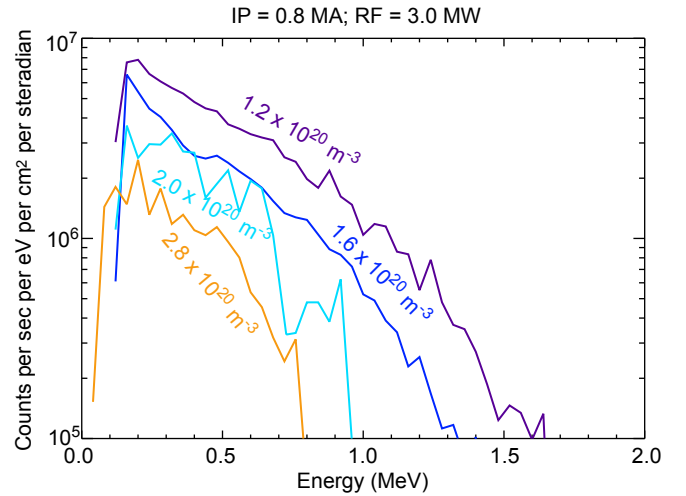


FIG. 6: Fast-ion distributions at the CNPA detector for various electron densities at 3 MW RF power and 0.8 MA plasma current.

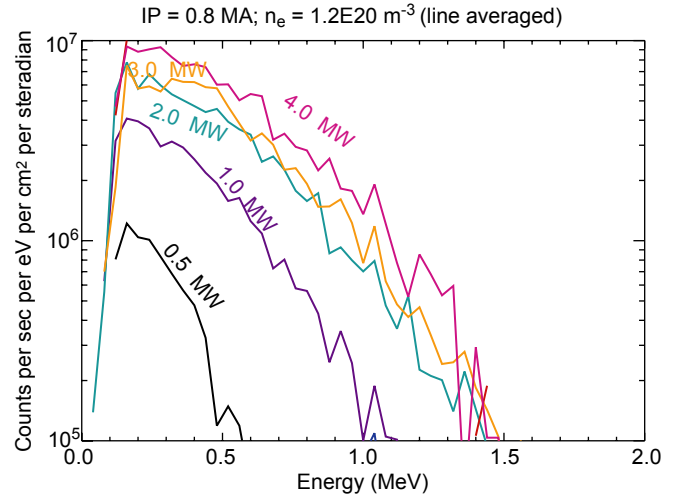


FIG. 7: Fast-ion distributions at the CNPA detector for various RF powers at line-averaged n_e of 1.2×10^{20} and 0.8 MA plasma current.

[20, 21]. Furthermore, sawtooth losses are most likely to occur for passing ions with turning-points near the trapped-passing boundary [16]. Passing particles are not detectable with the CNPA due to geometry constraints. As such, we do not expect sawteeth to modify the profiles of the fast-ions that are in the sightlines of the CNPA, however, they may redistribute particles in other areas of velocity space. The immunity to sawteeth is apparent in Figure 10 where we consider all fast-ion events over many sawtooth periods binned to the relative times during the sawtooth cycle, t/t_s . The results for one discharge are plotted and show no variation of fast-ion counts relative to t/t_s . No dependence on sawtooth cycle is found re-

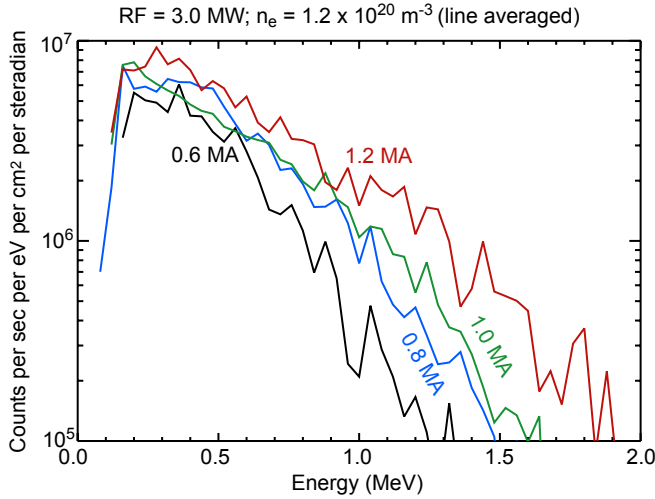


FIG. 8: Fast-ion distributions at the CNPA detector for various plasma currents at line-averaged n_e of 1.2×10^{20} and 3.0 MW RF Power.

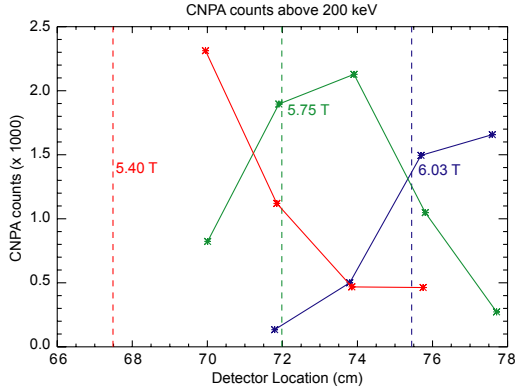


FIG. 9: Count rates for CNPA detectors as a function of toroidal field. Each starred symbol is a different detector location. Each curve represents the count rates for each detector for a single discharge at the indicated toroidal field value.

ardless of the height of the sawtooth crash, the length of the sawtooth period, or any other plasma parameters such as plasma current, electron temperature or electron density.

IV. ESTIMATION OF THE DISTRIBUTION IN THE PLASMA

The flux of charge-exchanged neutrals to the detector is the convolution of the neutralization probability times the probability of escaping, integrated along a line

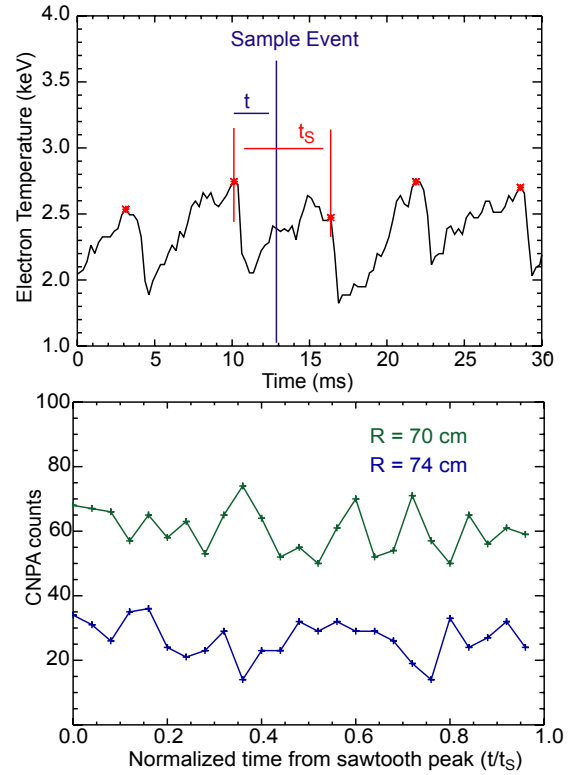


FIG. 10: Fast-ion events are measured relative to a sawtooth time (top). Total fast-ion events between 200 keV and 2 MeV are plotted vs the relative time during a sawtooth cycle (bottom).

of sight, and can be written as,

$$\Gamma(W) dW = v_0^2 dv_0 \epsilon \times \int_l A(x, \vec{v}_0) f_{fi}(x, \vec{v}_0) \left[\sum_s \sigma(v_0) v_0 n_s(x) \right] dl. \quad (1)$$

Here the flux is given as particles per unit energy per second between energies W and $W + dW$. v_0 represents the speed of a particle with energy W , $A(x, \vec{v}_0)$ is a unitless factor that measures the probability a fast neutral will exit the plasma without reionizing, ϵ is the etendue of the diagnostic, f_{fi} is the fast-ion distribution, and the last term $\sum_s \sigma(v_0) v_0 n_s(x)$ represents the number of neutralizations per second summed over all electron donor species. In order to estimate the effective temperature, T_{eff} , of the fast-ion distribution it is necessary to make some assumptions on both the distribution of fast-ions and the densities of the various electron donor species.

The location of the fast-ions in the plasma affects two terms in Equation 1, the probability of escape, and the probability of neutralization. Furthermore, one of the candidate processes for neutralization, charge-exchange (CX) with hydrogen-like boron (B^{4+}), does not have ex-

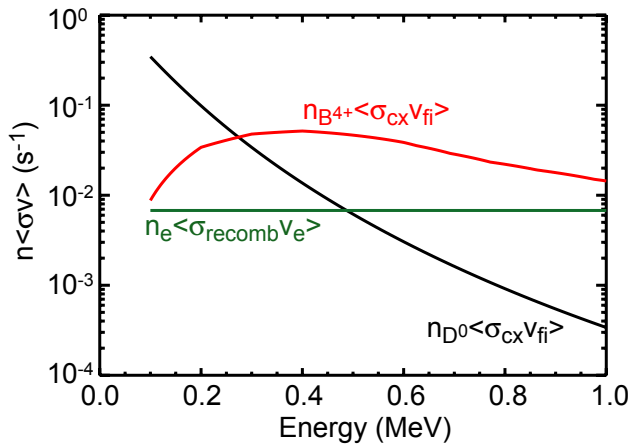


FIG. 11: Expected reaction rates for charge exchange with neutral deuterium and hydrogen-like boron and electron recombination are plotted vs. fast-ion energy.

perimentally measured cross-sections in the relevant energy range, and estimates are provided from the Second Born Approximation [22] adjusted to agree with more advanced theoretical models by Winter [23, 24]. Impurity boron in C-Mod is typically on order 1% of n_e [25]. B^{4+} density is estimated with a coronal equilibrium calculation. Intrinsic neutral deuterium estimates are obtained using the FRANTIC module in TRANSP simulations [26] with confinement times that produce edge neutral densities in agreement with [27]. Cross sections for neutral deuterium are obtained from [28]. Lastly, recombination rates are taken from [29], valid for the region where the fast-ion velocity is much less than the electron velocity. The reaction rates using these estimates for cross-sections and densities for a typical C-Mod plasma are shown in Figure 11. Charge-exchange with B^{4+} is likely to be the dominant neutralization process for fast-ions between 300 keV and 1 MeV.

Some fraction of the fast neutrals will reionize before exiting the plasma. This factor lowers the total number of fast neutrals that are likely to reach the detector. The probability of ionization can be obtained using ionization cross-sections by Janev [30]. These cross-sections include both electron impact ionization, ion-impact ionization, charge-exchange with impurities, and multi-step processes. For typical C-Mod parameters the probability of escaping from the core of the plasma without reionization is above 75% for fast-ions above 200 keV.

V. EFFECTIVE TEMPERATURES OF THE FAST-ION DISTRIBUTION

Using the simplification that fast-ions originate from a single location in physical space, we can write the distri-

bution function in terms of the detector signal,

$$f_{fi}(v_0) = \frac{\Gamma(W)dW}{\sum_s [n_s \sigma v_0] A(W) \epsilon L_c v_0^2 dv_0}. \quad (2)$$

Here L_c represents the length scale of the region over which the fast-ions are formed. This does not vary between discharges and therefore does not affect the calculation of the effective temperature. Because the relative concentrations of neutral deuterium and boron are poorly known experimentally, and tend to vary across multiple discharges during a campaign, for this analysis we will assume that only charge-exchange with hydrogen-like boron occurs, and we fit the distribution function between 300 keV and 1 MeV. This range represents the energies where charge-exchange with B^{4+} is dominant for the majority of reasonable relative density concentrations.

We find that in this range of energies there is little difference in the quality of fit between a simple exponential fit and a fit using a Stix distribution. This differs from the low-energy, low-power analysis done by Tang [19]. In Tang's results the Stix fit produced improved agreement over the exponential fit. The simple exponential fit is easier to interpret and is thus used for the analysis. The distribution function is modeled as,

$$\frac{f(W)}{T_{\text{eff}}} = \frac{df}{dW}. \quad (3)$$

In Figure 12, T_{eff} is plotted as a function of plasma parameters. Here we see verification that there is a strong scaling of fast-ion temperature with density and plasma current, and a weak scaling with RF power.

VI. DISCUSSION OF RESULTS

In this section we discuss the empirically measured dependencies of the fast-ion distribution on plasma current and RF power. First, we examine some of the possibilities to explain the dependence on plasma current. At low currents it is possible that larger banana widths cause prompt losses of fast-ions thus depleting the high-energy region of the fast-ion distribution. This explanation cannot be rejected based solely on the experimental evidence presented here. However, we find a significant reduction of fast-ions below 1 MeV. It is expected that the fast-ions that are viewable by the CNPA in this energy range are well confined, and simulation results confirm this prediction [17]. Additional experimental evidence on whether ions on lost orbits are important for the lower observed tail temperatures at low currents will be available with the installation of a new Fast Ion Loss Detector [31] that will be operational in 2012.

Another explanation of the current dependence could be higher neo-classical diffusion of fast-ions at lower currents. This explanation is similar to the prompt losses

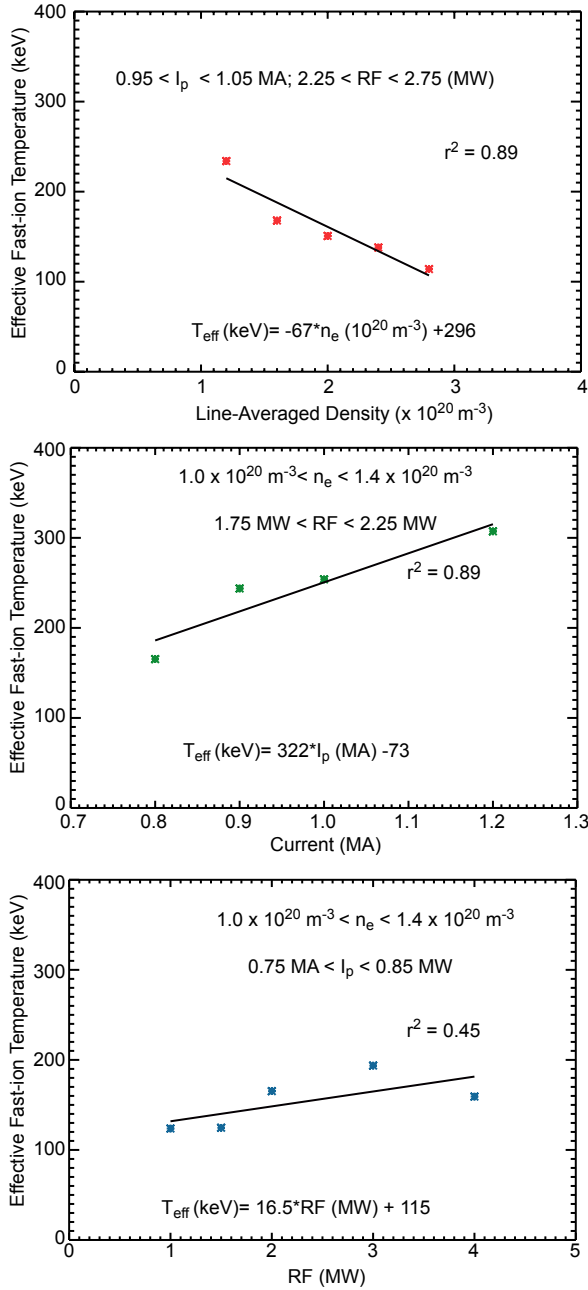


FIG. 12: Calculated effective temperatures of the fast-ion tail as a function of electron density (top), plasma current (middle), and RF power (bottom). Equations for the linear trendlines and r^2 goodness of fit values are also shown.

described above. However, instead of ions being removed from the plasma altogether, they diffuse out of the viewing sightlines through a current-dependent neo-classical diffusion operator. This effect cannot be determined with a loss detector, but may be testable with advanced simulations. In addition it is possible that there is a current dependent anomalous diffusion term that provides some transport of fast-ions at low current. However, anoma-

lous diffusion is usually a poor choice for resolving discrepancies at high energies because very high energy ions will average over microturbulence regions and thus be immune to their effects [32].

A third explanation to explain the trend with plasma current is the possible dependence of the wave-absorption on magnetic geometry. Examining this dependency of the wave damping on magnetic geometry requires the use of advanced simulation techniques [33] that can model the wave fields taking into account the magnetic geometry and the perturbed minority ion distribution. A dedicated experiment to produce plasmas suitable for simulations in which we measured the effect of plasma current on the fast-ion distribution has been performed and will be presented in the forthcoming paper on simulation results [17].

The observed saturation of fast-ion temperature as a function of RF power is also not well understood. Previous results with second harmonic heating on JET indicate that the fast-ion distribution from ICRF heating can be strongly affected by Finite Larmor Radius (FLR) effects if $k_{\perp} \rho_i \geq 1$, where k_{\perp} is the perpendicular wave number of the ICRF wave, and ρ_i is the ion gyroradius. At high values of $k_{\perp} \rho_i$ the RF diffusion coefficient (D_{RF}) can go to zero, essentially setting an upper limit to fast ion energy. Indeed this was the result seen by Mantsinen et al. in JET second harmonic cases, [34, 35]. The values of $k_{\perp} \rho_i$ and D_{RF} for C-Mod are plotted in Figure 13. We have assumed the following parameters: $n_e = 1 \times 10^{20} \text{ m}^{-3}$, $B = 5.3 \text{ T}$, and $f_{\text{RF}} = 78 \text{ MHz}$. Then, we can express k_{\perp} at the resonance location as,

$$k_{\perp}^2 = 2 \left[\frac{\omega_{\text{RF}}}{v_A} \left(\frac{1 - n_H/n_e}{3} + \frac{n_H/n_e}{4} \right) - k_{\parallel}^2 \right], \quad (4)$$

where v_A is the Alfvén velocity [36]. The parallel wave number, k_{\parallel} is determined by machine parameters, and can be expressed as the toroidal wave number, n_{ϕ} over the major radius. Here, n_{ϕ} is taken to be 10 [13]. Using typical C-Mod parameters, $k_{\perp} \approx 40 \text{ m}^{-1}$. For the fundamental minority heating case, the RF Diffusion coefficient is proportional to,

$$D_{\text{RF}} \propto |J_0(k_{\perp} v_{\perp} / \omega_c) + (E_- / E_+) J_2(k_{\perp} v_{\perp} / \omega_c)|^2, \quad (5)$$

where the values for v_{\perp} and ω_c are evaluated at the resonance location. Hydrogen minority fractions in C-Mod are typically around 5-10%. We use $E_- / E_+ = 3$ as a lower limit for the ratio of electric field polarizations at the fundamental resonance, noting that this is a lower bound for the polarization ratio. Higher values for E_- / E_+ will raise the cutoff energy for the RF Diffusion coefficient [36].

From Figure 13 we see that even though the values of $k_{\perp} \rho_i \geq 1$ for energies above about 1 MeV, the diffusion coefficient does not decrease in value until $\sim 4 \text{ MeV}$, and does not reach 0 until almost 20 MeV. Therefore, it is unlikely that we are seeing a steep falloff due to small values of D_{RF} over the energy ranges of interest. Never-

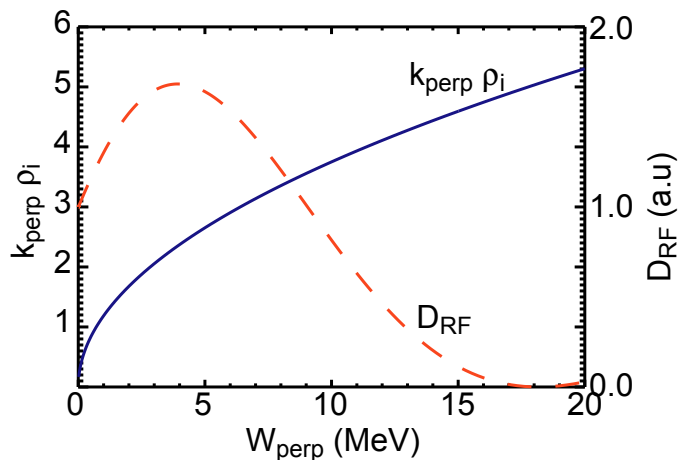


FIG. 13: Value of $k_{\perp}\rho_i$ (blue, solid) is plotted for typical C-Mod parameters. Also plotted is a normalized value of D_{RF} (red, dashed) over the same energy range.

theless, the high values of $k_{\perp}\rho_i$ preclude the use of simple theoretical models such as the Stix model, and would require modeling techniques that are accurate to all orders of $k_{\perp}\rho_i$. This modeling has been carried out and will be the subject of a future publication [17].

Additionally, in simulations of a JET-like plasmas Carlsson et al. found that wave-induced spatial diffusion would move resonant ions radially outward along the resonance until the large banana orbits caused the ions to leave the plasma [37]. Furthermore this effect increases superlinearly with ICRF power, providing a possible mechanism for suppression of highly energetic ions at high RF powers. Instead, the RF power would be deposited on lower energy ions causing an increase in density at the lower energies, a trend that is present in the experimental data (Fig 7).

Another possible explanation for the RF power dependence is enhanced Doppler broadening of the resonance layer, such that, after a certain tail-temperature has been reached, the power begins damping over a broader spatial region. It is possible that this result may not extrapolate to other contemporary devices or ITER, which cannot reach the same power per particle ratios.

The dependency on RF power warrants further research. Results from additional radial channels were not available for this paper due to much reduced signal-to-noise levels on these channels resulting in very poor statistics. However, with data from future campaigns, analyses for additional radial channels should become

available. Furthermore, a dedicated experiment to study the effect of RF power on the fast-ion distribution has not yet been performed. Such an experiment could help shed more light on the saturation region. Also, additional experimental data is desirable in the low-current and low-power regime, both of which are difficult to measure due to reduced signal levels.

VII. CONCLUSION

New diagnostic capability on Alcator C-Mod has allowed for the first ever systematic measurements of the fast-ion distribution for plasmas in the high RF power density regime. The diagnostic can measure particles between 200 keV and 2 MeV, and provides the first measurements showing the existence of fast-ions above 500 keV on C-Mod.

In the high power density regime we find interesting dependencies of the effective temperature and density of the high energy tail of the minority distribution on plasma current and injected RF power. We find that there is a strong dependency of the effective temperature on plasma current, implying that the magnetic topology of the plasma has a strong effect on the fast-ion tail. We also find a saturation of the tail temperature at RF powers above 2 MW, with higher injected powers not showing an increase in the tail temperature, although there is some increase in the tail density.

The strong current dependence of the fast-ion distribution, and the saturation with RF power have not been reported on other tokamaks. It is possible that both the dependence on plasma current and the dependence on RF power are only present in the high power density regime, and thus would not be present on other devices. However, even if the high power regime is not achievable, it may be possible to obtain agreement with other machines that use minority heating (JET, ASDEX etc.) in the low power density regime. We can then attempt to determine the importance of power density in the scalings presented here.

Acknowledgments

This work supported by USDOE awards DE-FC02-99ER54512.

References

-
- [1] WEYNANTS, R., ICRF review: From ERASMUS to ITER, RF Power in Plasmas, Gent, Belgium, 2009.
 - [2] STIX, T., Nuclear Fusion **15** (1975) 737.
 - [3] ERIKSSON, L.-G. et al., Nuclear Fusion **29** (1989) 87.
 - [4] ERIKSSON, L.-G. et al., Nuclear Fusion **33** (1993) 1037.
 - [5] ROQUEMORE, A. L., Review of Scientific Instruments **56** (1985) 1120.
 - [6] KISLYAKOV, A. I. et al., Fusion Engineering and Design

- [7] **34-35** (1997) 107, Fusion Plasma Diagnostics.
LEE, W. et al., Plasma Phys. and Controlled Fusion **45** (2003) 1465.
- [8] KRASILNIKOV, A. V. et al., Review of Scientific Instruments **70** (1999) 1107.
- [9] MURAKAMI, S. et al., Nuclear Fusion **46** (2006) S425.
- [10] VERBEEK, H. et al., Journal of Nuclear Materials **196-198** (1992) 1027.
- [11] SHINOHARA, K. et al., Review of Scientific Instruments **75** (2004) 3640.
- [12] TANG, V. et al., Rev. of Sci. Inst **77** (2006).
- [13] BONOLI, P. et al., Fus. Sci. and Tech. **51** (2007) 401.
- [14] KOROTKOV, A. et al., Nuclear Fusion **37** (1997) 35.
- [15] KIPTILY, V. et al., Nuclear Fusion **45** (2005) L21.
- [16] KIPTILY, V. et al., Nuclear Fusion **49** (2009) 065030.
- [17] BADER, A., *Experimental Measurements and Numerical Modeling of Fast-ion Distributions on the Alcator C-Mod Tokamak*, PhD thesis, MIT, Department of Nuclear Science and Engineering, 2011.
- [18] ROST, J. C., *Fast Ion Tails during Radio Frequency Heating on the Alcator C-Mod Tokamak*, PhD dissertation, MIT, Department of Physics, 1998.
- [19] TANG, V. et al., Plasma Physics and Controlled Fusion **49** (2007) 873.
- [20] MUSCATELLO, C. M. et al., Plasma Physics and Controlled Fusion **54** (2012) 025006.
- [21] KOLESNICHENKO, Y. et al., Nuclear Fusion **40** (2000) 1325.
- [22] MACEK, J. et al., Phys. Rev. A **26** (1982) 250.
- [23] WINTER, T. G., Phys. Rev. A **69** (2004) 042711.
- [24] WINTER, T. G., Phys. Rev. A **33** (1986) 3842.
- [25] R. M. MCDERMOTT, B. LIPSCHULTZ, J. H., Phys. of Plas. **16** (2009).
- [26] TAMOR, S., Journal of Computational Physics **40** (1981) 104.
- [27] HUGHES, J. W. et al., **13** (2006) 056103.
- [28] R.K JANEV, J. S., Suppl. to Nuc. Fus. **4** (1993).
- [29] HUTCHINSON, I., *Principles of Plasma Diagnostics, 2nd ed.*, Cambridge Univ. Press, 2002.
- [30] R.K JANEV, C.D. BOLEY, D. P., Nuc. Fus. **29** (1989).
- [31] FISHER, R. K. et al., Review of Scientific Instruments **81** (2010) 10D307.
- [32] ANGIONI, C. et al., Physics of Plasmas **15** (2008) 052307.
- [33] E.F. JAEGER, L.A. BERRY, E. D., Phys. of Plas. **9** (2002).
- [34] SALMI, A. et al., Plasma Physics and Controlled Fusion **48** (2006) 717.
- [35] MANTSINEN, M. et al., Nuclear Fusion **39** (1999) 459.
- [36] PERKINS, F. W., Plasma Science, IEEE Transactions on **12** (1984) 53.
- [37] CARLSSON, J. et al., Nuclear Fusion **37** (1997) 719.